Spatial extent of the Dzyaloshinskii-Moriya interaction at metallic interfaces

William Legrand, Yanis Sassi, Fernando Ajejas, Sophie Collin, Laura Bocher, Hongying Jia, Markus Hoffmann, Bernd Zimmermann, Stefan Blügel, N. Reyren, et al.

published in
Phys. Rev. Materials 6, 024408 (2022)
https://doi.org/10.1103/PhysRevMaterials.6.024408

How interfacial is the Dzyaloshinskii-Moriya interaction at metallic interfaces?

William Legrand,[1,*] Yanis Sassi,[1] Fernando Ajejas,[1] Sophie Collin,[1] Laura Bocher,[2] Hongying Jia,[3] Markus Hoffmann,[3] Bernd Zimmermann,[3] Stefan Blügel,[3] Nicolas Reyren,[1] Vincent Cros,[1,†] and André Thiaville[2]

[1] *Unité Mixte de Physique, CNRS, Thales, Université Paris-Saclay, 1 Avenue Augustin Fresnel, 91767, Palaiseau, France*
[2] *Université Paris-Saclay, CNRS, Laboratoire de Physique des Solides, 91405 Orsay, France*
[3] *Peter Grünberg Institut and Institute for Advanced Simulation, Forschungszentrum Jülich and JARA, 52425 Jülich, Germany*

(Dated: January 12, 2022)

We experimentally investigate the range of the Dzyaloshinskii-Moriya interaction (DMI) occurring at magnetic interfaces within metallic heterostructures. To this aim we perform Brillouin light scattering spectroscopy on a set of Co-based, asymmetric metallic heterostructures, incorporating atomically thin continuous films obtained by room-temperature sputtering, and of identical orientation and quality. We thus get access to the intrinsic dependence of the interfacial DMI and other magnetic interactions on the thickness of the non-magnetic layer adjacent to Co, which is chosen among Pt, Ru and Au. Notably, we observe that a robust DMI is already generated by as few as two atomic planes of Pt, and that interfacial DMI can be efficiently suppressed by a dusting of Ru equivalent to a single atomic plane coverage. These results point directly towards a mechanism where DMI is generated within the two first atomic planes away from the interface, in agreement with first-principles calculations. This locally generated DMI is however likely to be modulated by more distant atoms in the case of strain effects. The short-range aspect of the interfacial DMI opens up the synthesis of dense magnetic multilayers, allowing for a strong interfacial DMI even with very thin layers, which can be further tuned by strain engineering.

I. INTRODUCTION

Since its discovery in the context of interfacial systems [1, 2], the Dzyaloshinskii-Moriya interaction (DMI) [3, 4] has become a prominent constituent of the design of magnetic multilayers [5–7]. Be it for increasing the maximal current-induced velocity of magnetic domain walls [8] or for reducing the minimal size of stable magnetic skyrmions [9], among many other examples, maximizing the strength of the DMI often provides (but not always, see, e.g., [10]) a clear advantage over when the DMI is weak or absent. This has led to a widespread use of interfacial DMI in several types of research-stage magnetic devices [11, 12]. As the electronic mechanisms involved in interfacial DMI generation begin to be unveiled by theoretical works [13–17], their understanding in actual multilayers remains so far incomplete [18]. No clear direction appears as to how the DMI of multilayer systems could be improved beyond the best results to date. This provides a strong motivation to investigate into more details the DMI in interfacial systems with layers that are typically one nanometer-thick [19–41], composing these multilayers.

For a large majority of the common magnetic materials, which do not incorporate a suitable break of symmetry in crystalline structure or composition, or even adopt amorphous phases, the DMI is not naturally present. Therefore when dealing with these materials, the most common way to nevertheless obtain a significant DMI is to harness the electronic effects occurring at the interfaces between adjacent layers of different composition, which we refer to as interfacial DMI. After the broad experimental survey that has been conducted over the recent years, looking for combinations of elemental metals, alloys and/or oxides providing a robust DMI, the Pt/Co pair has remained favored, and the only solution to obtain the largest DMI strengths. Its interfacial DMI parameter D_s reaches values up to around $1.5\,\mathrm{pJ\,m^{-1}}$ [18], a value that can be slightly enhanced when the Pt/Co interface is combined with a Co/AlO_x [20] or Fe/Ir [42] interface at the opposite side of the ferromagnetic layer. Following an alternative to the promising approach of investigating new types of materials or heterostructure combinations [41, 43–46], we aim here to learn from a thorough investigation of the interfacial DMI in conventional Pt/Co-based metallic systems.

In particular, several works have reported diverging observations concerning how the DMI depends on both thickness and structure of the layers that are adjacent to the ferromagnetic layer. First-principles models point out a strongly localized origin for the DMI [13, 16, 47]: even if the detailed contributions of each atomic plane may vary, all these works predict that an essential part of the DMI should originate from the first or first two atomic plane(s) away from the interface. In contrast with this finding, several experiments report a pronounced dependence of the DMI on the thickness of the adjacent layers, up to 2 nm, thus of the order of 10 atomic planes [25, 27, 32].

In the present work, we intend to scrutinize the characteristic length associated with the build-up of the DMI at the interface between a ferromagnet (FM) and a metal.

* william.legrand@cnrs-thales.fr
† vincent.cros@cnrs-thales.fr

The key issue here is to understand whether atoms from off-nearest planes in the non-magnetic layers influence significantly the interfacial DMI. Such understanding shall determine whether it is possible to modulate the DMI through the insertion of additional layers farther from the interface. We also intend to compare this potential effect on the DMI with that on the other magnetic properties and interactions in these systems, namely, Heisenberg exchange interaction, magnetic anisotropy, and saturation magnetization. We may already note that similar considerations concerning the thickness of the ferromagnetic layer itself appear to bring relevant results [40]. Stemming from the interfacial origin of the DMI, its amplitude is expected to scale as the inverse of the thickness of the magnetic layer [19, 20]. However, below a certain threshold the DMI drops rapidly, at a thickness that could be assigned to a characteristic length for DMI build-up on the side of the FM; for instance, this limit thickness is 0.4 nm to 0.6 nm in the case of Co [40], a value probably related to various other material properties as well, such as intermixing or roughness, in addition to purely electronic effects.

In the following we focus on how thin metallic layers of different thicknesses (0.1 nm to 3.5 nm) incorporated at the interface between an FM and a non-magnetic layer, of fixed thicknesses, influence the DMI. Antisymmetric exchange (DMI) as well as symmetric exchange (Heisenberg) constants are determined by Brillouin Light Scattering (BLS) experiments performed on thoroughly characterized metallic heterostructures. By relying on a template seed heterostructure with well-controlled interfacial texture, we are able to isolate the relevant intrinsic thickness dependence among the other mechanisms also affecting the DMI, such as changes in crystalline structure or interfaces quality. This allows us to analyze in a consistent way the results obtained from fine-resolved thicknesses series (with 0.1 nm increments, or about half an atomic plane) of heterostructures having different layer compositions. The main observations are that 2 atomic planes of Pt are enough to enable almost fully the DMI at the Co/Pt interface, and that conversely, 1 or 2 atomic planes of a metal other than Pt inserted between Co and Pt are enough to prevent DMI generation at this interface. In addition, the non-equivalent DMI contributions observed for the two interfaces present in Pt/Co/Pt point toward a strain modulation effect. These experimental results are supported by first-principles calculations performed for the cases of Pt/Co/Ru/Pt and Pt/Co/Pt/Au heterostructures, which together confirm the short range of the electronic effects causing interfacial DMI in these systems.

II. EXPERIMENTS AND METHODS

A. Deposition of metallic interfacial DMI systems

We investigate different series of metallic heterostructures, which all have in common an identical bottom part, made of a seed layer and FM, of composition Ta(10)/Pt(8) and Co(1.7), respectively. The numbers in parentheses indicate the thickness of each layer in nm, as will be the case for all experimental heterostructures described hereafter. All samples are deposited by d.c. magnetron sputtering on thermally oxidized silicon wafers with a nominal thickness of 290 nm of SiO_2, which is important for the optimization of the BLS signal [48]. All the studied systems are either ended or additionally capped by Pt or Au layers, 3 nm or thicker, in order to prevent oxidation. For each sample, the saturation magnetization M_s of the Co layer at room temperature is measured by SQUID magnetometry, and its effective magnetic anisotropy is determined using an alternating gradient field magnetometry (AGFM) setup, which confirms an in-plane effective magnetic anisotropy for all these samples with a Co(1.7) layer. Note that the Co magnetic layer is chosen thick enough to allow neglecting electronic interference effects between its bottom and top interfaces, usually found in thinner layers.

B. Importance of buffer template layer

The choice of a single combination of seed and magnetic layers, Ta/Pt/Co, with fixed thicknesses, imposes an fcc structure propagating from the dominantly (111)-oriented granular texture at the seed Pt surface. This ensures that the growth of the layers deposited above initiates under consistent conditions. In addition, by keeping a constant FM layer thickness, the atomic configuration presented by the Co at its top interface is expected to remain identical. The actual thicknesses are verified specifically on one multilayer, nominally Ta/Pt(8)/Co(1.7)/Ru(3.2)/Pt(3.0), by fitting low-angle X-ray reflectivity measurements presented in Fig. 1a, resulting in best-fit thickness results of Pt $(7.84 \pm 0.02\,\text{nm})$/Co $(1.62 \pm 0.01\,\text{nm})$/Ru $(3.13 \pm 0.01\,\text{nm})$/Pt $(3.00 \pm 0.01\,\text{nm})$. The low-angle X-ray reflectivity measurements also confirm low interface roughnesses, with best-fit roughness results around 0.2 nm for Pt and 0.45 nm for Co and Ru, corresponding to a long-range modulation of interface heights.

To further assess the crystalline quality, interfaces and interdiffusion properties of the multilayers, we additionally acquire high-angle annular dark-field (HAADF) images in scanning transmission electron microscopy (STEM) performed onto cross-sectional lamellas ($\approx$ 80–100 nm), from multilayers of a series Ta(10)/Pt(8)/Co(1.7)/Ru(t_{Ru})/Pt(3), with $t_{Ru} = 0$, 0.5, and 0.9 nm (same deposition as later studied samples). The layers of interest consist of textured polycrystalline

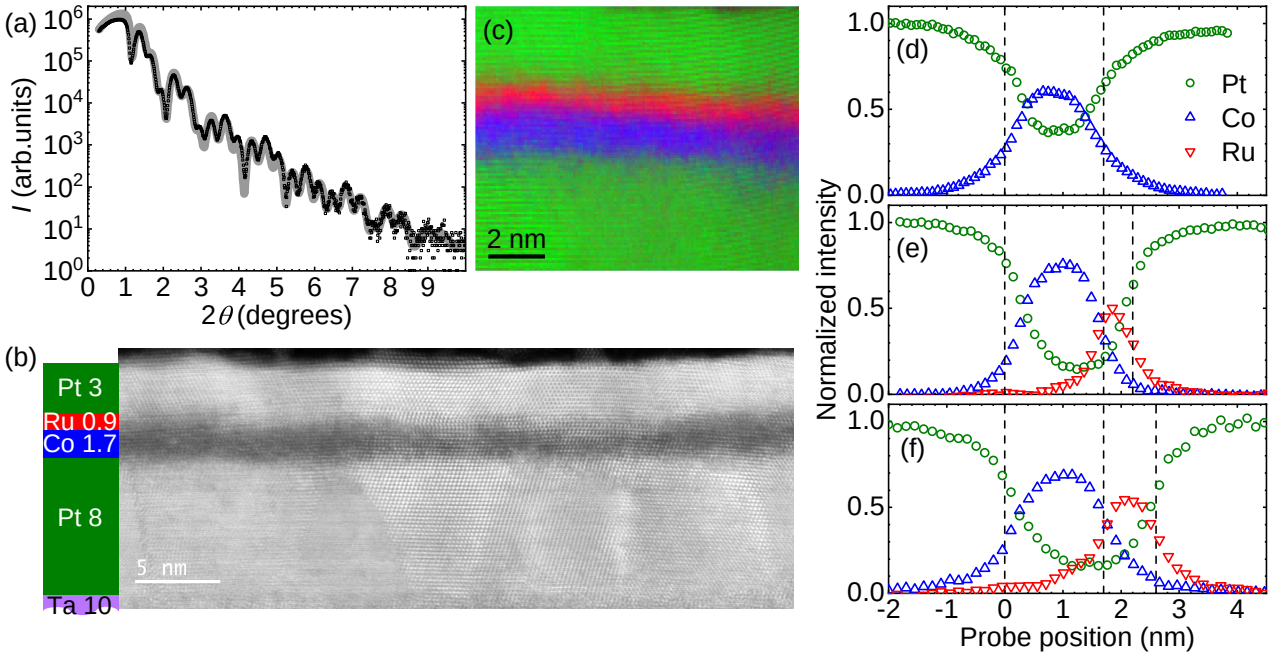

FIG. 1. Structural characterization of the multilayers. **a**. X-ray reflectivity of a Ta(10)/Pt(8)/Co(1.7)/Ru(3.2)/Pt(3) (where numbers indicate layer thicknesses, in nm) heterostructure (symbols) and a fit (thick line) indicative of a low layer roughness, measured with a Cu K_α source. **b**. Typical HAADF-STEM image of a Ta(10)/Pt(8)/Co(1.7)/Ru(0.9)/Pt(3) heterostructure displaying grains of lateral dimensions of 5–10 nm. The structure with its nominal thicknesses is drawn to scale on the left of the micrograph. Darker area above the structure corresponds to additional Pt deposited for FIB sample preparation. **c**. EELS maps (combined in a single false colors map) at Pt-$M_{4,5}$ (green), Co-$L_{2,3}$ (blue) and Ru-M_3 (red) edges, acquired in a Ta(10)/Pt(8)/Co(1.7)/Ru(0.9)/Pt(3) multilayer displaying again well defined interfaces. **d–f**. Extracted elemental concentration profiles across Ta(10)/Pt(8)/Co(1.7)/Ru(t_{Ru})/Pt(3) for $t_{\mathrm{Ru}} = 0$ (d), 0.5 (e), and 0.9 nm (f). The probe position axis is oriented along growth direction and is zeroed at the bottom Pt/Co interface. Nominal interface positions according to thicknesses are indicated by the dashed lines. The curves correspond to an integration over the slab thickness ($\approx$ 80–100 nm, *i.e.*, several grains) and a width of 2 nm. The Ru layer interfaces are sharper than the Pt/Co/Pt ones.

grains with a typical size of 5 to 10 nm in width, alternating with different crystal orientations. The Pt layers can be clearly identified by the higher contrast in the HAADF image, while Co/Ru layers are distinguishable by their lower contrasts. All investigated Pt/Co/Ru/Pt multilayers present homogeneous layer thicknesses for a given Ru thickness, continuing along the film, observed at various locations over a long distance much greater than 500 nm (Supplemental Material). The fcc stacking of the bottom Pt layer retains a good crystal quality propagating in the upper Co, Ru and Pt layers, with the same crystal orientation within each columnar grain (Fig. 1b, see also additional images and methodology in Supplemental Material). This aspect proves crucial as it avoids changes in the orientation and quality of the interfaces between Co and the other metallic layers investigated, to better access the intrinsic evolution of the DMI with the thickness of the adjacent layers.

The elemental distributions across the Ta(10)/Pt(8)/Co(1.7)/Ru(t_{Ru})/Pt(3) multilayers were further investigated by electron energy-loss spectroscopy (EELS), yielding element-specific maps (Fig. 1c) and the extracted profiles shown in Fig. 1d–f. For these EELS measurements, the probed edges are Pt-$M_{4,5}$ at 2122 eV, Co-$L_{2,3}$ at 779 eV and Ru-M_3 at 461 eV (acquisition procedure detailed in Supplemental Material). The intensities of each elemental profile in Fig. 1d–f are normalized so that their sum provides 1 at every probe location, giving the relative atomic concentration profiles of each element for a constant probe volume. Thus, it allows us to evaluate possible chemical diffusion at interfaces. In all investigated multilayers, Pt remains significantly present within the Co/Ru layers, which most likely enables a better crystallinity propagation from the lower to the upper Pt layer. All Co layers fit to 1.65 ± 0.09 nm. In the absence of an Ru layer, the Pt/Co bottom interface is more abrupt than the top Co/Pt interface (Fig. 1d). By adding Ru to the top Co interface, both Pt/Co and Co/Ru interfaces are symmetric and abrupt (Fig. 1e,f), however Ru starts interdiffusing into the upper half of the Co layer. This Ru interdiffusion is particularly marked in the case of the thicker Ru layer (Fig. 1f) and may be induced by the sputtering deposition. It is noticeable that in Pt/Co/Ru/Pt, Pt tends to penetrate less in Ru at the top Ru/Pt interface than in Co at the bottom Pt/Co interface, with Ru

therefore acting as a diffusion barrier for Pt, even though also mixing slightly with Co. Overall, the interdiffusion remains moderate in Pt/Co/Ru/Pt. Even if varying the nature of the metal deposited above the Co layer may thus lead to nonequivalent levels of intermixing, it has been shown that moderate intermixing does not affect drastically the DMI at metallic interfaces [15]. The use of a buffer template system with good cristalline order thus favors a meaningful comparison of DMI constants obtained in all heterostructures, independent on their different compositions.

C. Brillouin light scattering

Symmetric exchange stiffness, Dzyaloshinskii-Moriya interaction strength and effective magnetic anisotropy are determined in the heterostructures by performing spectroscopy of thermally excited spin-waves, using a BLS setup in the backscattering configuration, at controlled room temperature. A linearly polarized laser light with wavelength 532 nm and power 10 mW is focused on a 30 µm-diameter spot (at normal incidence) in the center of a $10\times10\,\mathrm{mm}^2$ substrate, on which the magnetic heterostructure is deposited. The backscattered light is collected after a set of lenses and pinhole apertures for spatial filtering and analyzed in a JRS TFP-2 triple-pass tandem Fabry-Pérot interferometer with quarter wave antireflection optics. The BLS spectra are recorded at up to 5 incidence angles between 10 deg and 60 deg from normal incidence, and for the two opposite orientations of an in-plane field of 85 mT, large enough to saturate the in-plane magnetization in the Co layers. This field is obtained from permanent magnets which rotate together with the sample, ensuring a constant field for each sample orientation.

The BLS peaks are fitted by combined symmetric and antisymmetric Lorentzian peaks (see fitting function in Supplemental Material), which provides peak frequency and width for both anti-Stokes and Stokes conditions. The frequency shifts of the Stokes and anti-Stokes peaks obtained in the spectra are given in absolute value by the following approximate formulae [20–22, 49] valid for ultrathin films [50]:

$$f_{\mathrm{AS,S}} = f_0 \pm f_{\mathrm{DMI}}, \quad f_{\mathrm{DMI}} = \frac{\gamma}{\pi M_{\mathrm{S}}} k_{\mathrm{sw}} D \tag{1}$$

$$f_0 = \frac{\gamma\mu_0}{2\pi}\sqrt{\left[H_{\mathrm{ip}} + k_{\mathrm{sw}}^2 J + \xi(k_{\mathrm{sw}}t)M_{\mathrm{S}}\right]\left[H_{\mathrm{ip}} + k_{\mathrm{sw}}^2 J - \xi(k_{\mathrm{sw}}t)M_{\mathrm{S}} - H_{\mathrm{eff}}\right]} \tag{2}$$

$$\xi(x) = 1 - \frac{1-e^{-|x|}}{|x|} \tag{3}$$

where γ is the absolute value of the electron gyromagnetic ratio (with 2.17 for the g-factor of Co in our heterostructures), μ_0 the magnetic permeability of vacuum, H_{ip} the externally applied in-plane magnetic field, H_{eff} the effective magnetic anisotropy field (see definition below), $k_{\mathrm{sw}} = 4\pi\sin\theta/\lambda$ the wavevector of the spin-waves at the considered incidence angle θ for a laser wavelength λ, $J = 2A/(\mu_0 M_{\mathrm{S}})$ linking wavevector to an exchange field related to Heisenberg exchange A, and ξ accounts for the influence of dipolar interactions on the spin-waves. The frequency difference between both peaks is thus proportional to the parameter D of the DMI .

The dependence of the peak positions on the wavevector of the spin-waves is then analyzed jointly for both directions of the external in-plane field. Both A and effective anisotropy field H_{eff} can be determined by fitting the angular dependence of $f_{\mathrm{AS}}(k_{\mathrm{sw}}) + f_{\mathrm{S}}(-k_{\mathrm{sw}}) = 2f_0(k_{\mathrm{sw}})$, whereas the angular dependence of the frequency shifts $\Delta f = f_{\mathrm{AS}}(k_{\mathrm{sw}}) - f_{\mathrm{S}}(-k_{\mathrm{sw}}) = 2f_{\mathrm{DMI}}(k_{\mathrm{sw}})$, proportional to k_{sw}, provides an estimation of the DMI. The details of the measurements, together with fitting procedures, are described in the Supplemental Material. Importantly, this methodology allows for a precise determination, once added to magnetometry measurements, of all the micromagnetic parameters of importance for the design of magnetic multilayers [21, 51], as exemplified in section III. In particular, we obtain the evolution of the exchange stiffness parameter with the thickness of an Ru insertion layer in section V. When only the amplitude of the DMI is required (as in section IV), we simply measure the BLS spectra for both field directions at a single incidence angle of 60 deg.

All the uncertainties stated later on in the text are given at the ±1 standard deviation level, considering solely the errors in the fits originating from the counting statistics of the accumulated BLS spectra. All other uncertainties (thickness imprecision, measurement of M_{s}, etc.) are determined to be much smaller.

D. First-principles calculations

All first-principles calculations performed hereafter are based on density-functional theory (DFT). The structures of Pt[7]/Co[5]/Pt[n=0–7]/Au[7] and Pt[7]/Co[5]/Ru[m=0–7]/Pt[7] thin films with fcc-stacking and C_{3v} symmetry were simulated at FM states by fixing the in-plane lattice constant to the experimental value of Pt(111) (a = 2.77 Å). The numbers in brackets for systems studied by first-principles

calculations denote the number of atomic layers or monolayers (ML). Structural relaxations have been performed to determine the interlayer distances using the Vienna ab initio simulation package (VASP) [52, 53] employing the generalized gradient approximation (GGA) of Perdew-Burke-Ernzerhof (PBE) [54] for exchange and correlation effects in Pt[7]/Co[5]/Pt[n=0–7]/Au[7] and local density approximation (LDA) [55] in Pt[7]/Co[5]/Ru[m=0–7]/Pt[7] calculations. The magnetic properties were determined in the local density approximation (LDA), using the full-potential linearized augmented plane wave (FLAPW) method as implemented in the FLEUR code [56]. The energy dispersions $E(\mathbf{q})$ of spin spirals for these systems were obtained using a cutoff parameter for the basis functions of $\kappa_{\max} = 4.0\,\text{a.u.}$ and (24×24) k-points in the full two-dimensional Brillouin zone (BZ). The DMI was calculated using first-order perturbation theory [57] with (48×48) k-points in the full two-dimensional BZ on top of a scalar-relativistic spin-spiral calculation, as described in Refs. [16, 58]. The DMI values are extracted for the spin-spiral state of a general wave vector $\mathbf{q}||\hat{\mathbf{x}}$ and rotation axis $\hat{\mathbf{e}}_{\text{rot}} = \hat{\mathbf{y}}$. In order to be consistent with sign convention of a negative DMI in Pt/Co, all the computationally obtained D values shown in this paper are of opposite sign as those extracted from the calculations.

III. COMPARISON OF DIFFERENT TOP INTERFACES WITH Co

To obtain reference values for the magnetic parameters associated to the interfaces that we will consider later on, we first determine the magnetic properties of heterostructures varying the top interface with Co. It is chosen among Co/Ru (with additional Pt capping to prevent oxidation), Co/Au and Co/Pt, and in a regime where the non-magnetic top layers are thick, i.e., ≥ 10 atomic layers or ML, sufficient to prevent electronic interactions with farther atoms [15]. In this way, we aim to exclude any finer variations in the DMI that could come from atoms close to the interface and belonging to a different element.

By fitting the angular dependence of the central frequency $f_0(k_{\text{sw}})$ of the BLS peaks detected from these samples (see section II.C), we determine in these Co(1.7) ferromagnetic layers, $A = 23.0 \pm 0.6\,\text{pJ m}^{-1}$, $25.1 \pm 0.7\,\text{pJ m}^{-1}$ and $25.3 \pm 0.7\,\text{pJ m}^{-1}$, for a top interface with Ru, Au and Pt, respectively. Fitting the angular dependence of the frequency difference between anti-Stokes and Stokes BLS peaks leads to the following estimations of the DMI: $D = -0.747 \pm 0.015\,\text{mJ m}^{-2}$, $-0.686 \pm 0.017\,\text{mJ m}^{-2}$ and $0.069 \pm 0.017\,\text{mJ m}^{-2}$, for Ru, Au and Pt top layers, respectively. This corresponds, taking into account the 1.7 nm thickness of the present Co layers, to values of $D_{\text{s}} = -1.27 \pm 0.03\,\text{pJ m}^{-1}$, $-1.17 \pm 0.03\,\text{pJ m}^{-1}$ and $0.12 \pm 0.03\,\text{pJ m}^{-1}$, respectively, where the sign of D is defined as negative for a bottom Pt/top Co interface. The other magnetic parameters determined in these three systems are listed in Table I. The fourth line in Table I refers to a sample similar to the Pt/Co/Ru/Pt heterostructure described just above, but where Ru is capped by Au instead of Pt. The nearly identical values found for either Pt or Au above Ru indicate that the choice of capping layer far from the interface has a negligible influence on the magnetic properties of the system, which validates ≥ 10 ML as a thick top layer regime with no influence of additional layers. The reduction of A in the case of Co/Ru is likely due to the moderate interdiffusion of Ru into Co, as observed above in Fig. 1e,f, Ru being especially detrimental to the exchange interaction in Co [59]. Also, the onset of a significant proximity-induced magnetism at both Pt/Co and Co/Pt interfaces is evidenced by the larger apparent saturation magnetization M_{s} measured in Pt/Co/Pt than in the other heterostructures, see Table I.

In the case of Pt/Co/Ru, the ferromagnetic system exhibits a robust DMI, in excellent agreement with some previous results inferred from domains periodicity measurements [60], while the DMI in Pt/Co/Au [34] is found similar to that in Pt/Co/Ru. In combination with the previous finding that Co/Ru and Co/Au interfaces bring very small or even insignificant contribution to the DMI [31], these values of $|D_{\text{s}}| = 1.17$–$1.27\,\text{pJ m}^{-1}$ provide an estimate of the interfacial DMI at the bottom Pt/Co interface in our template system. The DMI measured in Pt/Co/Pt shows in contrast a drastically reduced value, and with opposite sign. For an ideal Pt/Co/Pt system, owing to the symmetry of the overall structure, an exact cancellation of the DMI would be expected as the negative contribution to the overall DMI from the bottom Pt/Co interface is matched by an equivalent positive contribution at the top Co/Pt interface. The positive D_{s} observed here in Pt/Co/Pt implies that the top Co/Pt interface contributes by a stronger amount than the bottom Pt/Co interface to the overall DMI of the magnetic system. This suggests that the configuration of both interfaces of Co with Pt are comparable but not identical [28]. This excess DMI in Pt/Co/Pt, with D_{s} about -10% of the value of Pt/Co, is most likely a consequence of either deposition-order induced strain asymmetry [61] and/or of slightly different levels of intermixing at both interfaces [15], as we discuss again below.

IV. EVOLUTION OF DMI WITH Pt INSERTION LAYER

In order to now evaluate the length scale over which metallic atoms contribute to the DMI, we investigate how a Pt layer, inserted in Pt/Co/Au between the Co layer and the Au top layer, affects the DMI, as function of its thickness. This series with Pt insertion layers follows composition Ta(10)/Pt(8)/Co(1.7)/Pt(t_{Pt})/Au(5), with t_{Pt} in the range of 0.1–3.5 nm.

Heterostructure	M_s (MA m^{-1})	H_{eff} (kA m^{-1})	K_u (MJ m^{-3})	A (pJ m^{-1})	D_s (pJ m^{-1})
Ta(10)/Pt(8)/Co(1.7)/Pt(3)	1.34 ± 0.03	$-\ 78.8 \pm 0.6$	1.06 ± 0.05	25.3 ± 0.7	0.12 ± 0.03
Ta(10)/Pt(8)/Co(1.7)/Au(5)	1.24 ± 0.02	-163.7 ± 0.8	0.84 ± 0.04	25.1 ± 0.7	-1.17 ± 0.03
Ta(10)/Pt(8)/Co(1.7)/Ru(3.2)/Pt(3)	1.19 ± 0.02	$-\ 69.3 \pm 0.5$	0.84 ± 0.04	23.0 ± 0.6	-1.27 ± 0.03
Ta(10)/Pt(8)/Co(1.7)/Ru(3.2)/Au(5)	1.18 ± 0.02	$-\ 65.6 \pm 0.6$	0.82 ± 0.04	21.0 ± 0.7	-1.26 ± 0.03

TABLE I. Magnetic properties determined for the thick capping layer systems.

We show, in Fig. 2, the evolution of the interfacial DMI parameter D_s with t_{Pt}. Although a thin dusting layer of Pt does not affect the DMI very significantly (points up to 0.2 nm in Fig. 2), the DMI then rapidly drops, reaching below 10% of the initial value already from $t_{Pt} = 0.65$ nm. A thin insertion layer made of Pt is therefore enough to enable a strong DMI at this top interface. To cancel the overall DMI in a heterostructure behaving as a symmetrical Pt/Co/Pt, without DMI, it requires $t_{Pt} \approx 1.0$ nm, even though the bottom Pt is 8 nm-thick. Beyond this thickness, a slightly positive DMI slowly builds up, as already mentioned.

The length scale for obtaining a significant interfacial DMI at the top interface is thus a couple ML only, short in comparison with the thickness of the FM layer. Even though, the interfacial DMI obtained from the top interface appears to progressively reinforce with the incorporation of additional atomic planes of Pt much beyond the interface, which we rather attribute to a strain modulation of the DMI generated locally at the interface [37], caused by these additional planes. We elaborate more on this aspect in section VI.

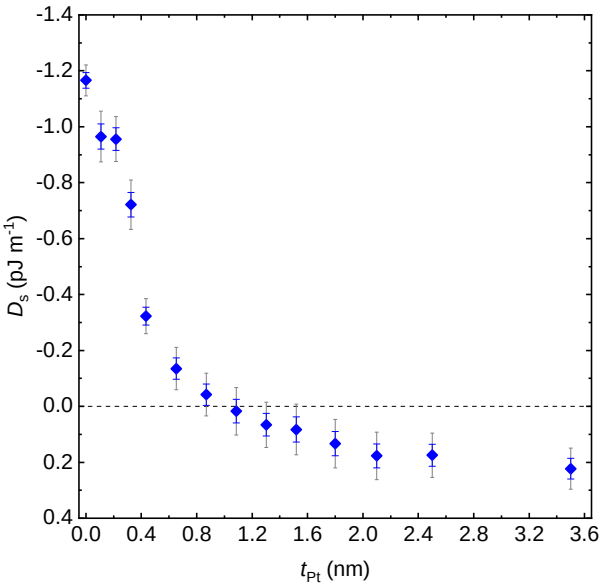

FIG. 2. Interfacial DMI constant D_s of Ta(10)/Pt(8)/Co(1.7) /Pt(t_{Pt})/Au(5) heterostructure as a function of Pt insertion layer thickness. Note the inverted vertical scale, which reflects the fact that we vary the thickness of the non-magnetic layer located at the top interface, and not at the bottom interface. For each point, the thick error bar represents the 1-σ confidence interval as extracted from the fit, owing to the BLS spectra accumulation statistics and the second thinner error bar represents the 2-σ confidence interval.

V. EVOLUTION OF MAGNETIC PARAMETERS WITH Ru INSERTION LAYER

To substantiate these findings, we now investigate how an Ru layer, inserted in Pt/Co/Pt between the Co and the top Pt layer, modulates the DMI and the other magnetic parameters, aiming to compare it with the case of Pt. This series with Ru insertion layers follows composition Ta(10)/Pt(8)/Co(1.7)/Ru(t_{Ru})/Pt(3), with t_{Ru} in the range of 0.1–3.2 nm.

We present in Fig. 3a the evolution of the interfacial DMI parameter with t_{Ru}. A limit value around $D_s \approx -1.3$ pJ m^{-1} is very rapidly attained, with more than 90% of this DMI built after only 0.3 nm, that is, less than 2 MLs. This shows that a thin dusting of Ru is already enough to screen the presence of Pt for generating DMI in Co, hence canceling it at this interface. The characteristic length scale for the suppression of the DMI by an Ru insertion layer is around the single atomic plane. This is consistent with previous first-principles calculations, which predict that Ru is indeed the most impactful among many elements for reducing DMI at the Co/Pt interface, where a dusting atomic coverage equivalent to about 1 ML of Ru reduces the interfacial DMI by a factor 3 [15].

Further looking at the plot, considering a 1-σ confidence interval around our data points, an oscillatory behavior of D_s with Ru thickness may be present, at $t_{Ru} = 0.7$ nm–1.1 nm in particular. However, these variations are not strong enough to remain conclusive when considering a 2-σ confidence interval, see inset of Fig. 3a. While finer variations of the DMI with additional Ru planes beyond the first atomic planes thus cannot be excluded (see also related discussion in section VI), it is observed here that these variations remain in practice negligible when the other interface is Pt/Co, being well below 10% of the total DMI value.

The evolution of the exchange stiffness parameter A with t_{Ru} is shown in Fig. 3b: after an initial drop of around 20% compared to the value in Pt/Co/Pt, attained for about 1 ML Ru, where A decreases from ≈ 25 pJ m^{-1} to ≈ 20 pJ m^{-1}, the value of A in Pt/Co/Ru/Pt recovers a level close to that in Pt/Co/Pt within about 4 MLs of

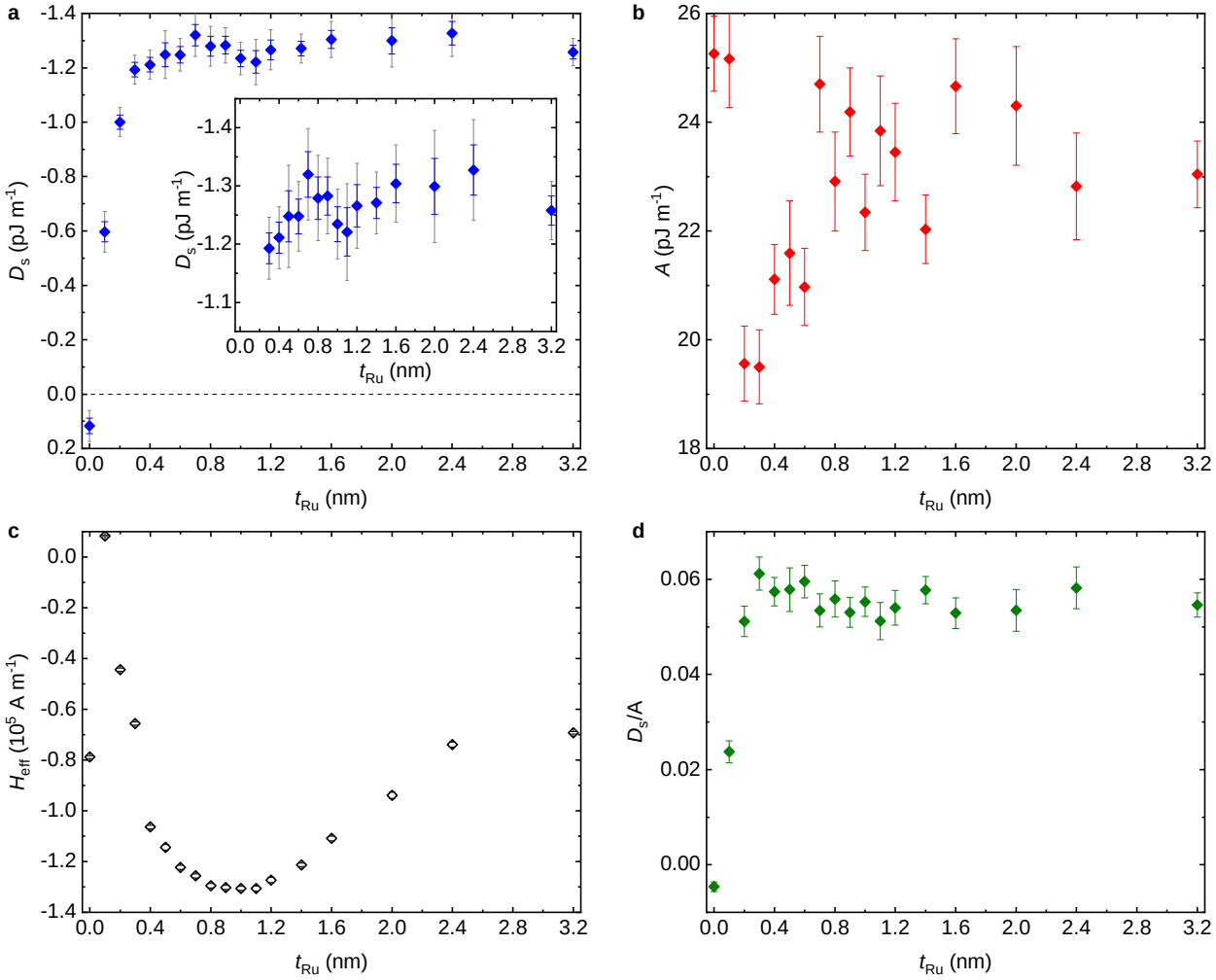

FIG. 3. Magnetic properties of Ta(10)/Pt(8)/Co(1.7)/Ru(t_{Ru})/Pt(3) heterostructure as a function of Ru insertion layer thickness: **a**. Interfacial DMI constant D_s (inset: magnified graph showing possible modulation behavior over 0.3 nm; note again the inverted vertical scale as in Fig. 2), **b**. Exchange stiffness constant A, **c**. Effective anisotropy field H_{eff} and **d**. Ratio of D_s/A. For each point, the error bar represents the 1-σ confidence interval of the parameters as extracted from the fits, owing to the BLS spectra accumulation statistics; in addition, for panel a only, a second set of thinner error bars represents the 2-σ confidence interval.

Ru.

In contrast, the effective magnetic anisotropy field H_{eff} evolves smoothly with t_{Ru}, with variations manifesting over a broader range of thicknesses than those of A, see Fig. 3c. The large relative variations for H_{eff} are due to the particular value of t_{Co}, chosen close to the spin-reorientation thickness, which is estimated to be around 1.5 nm in the present Pt/Co/Ru/Pt heterostructure. In this thickness regime, the shape anisotropy induced by dipolar interactions and generating an in-plane anisotropy field $-M_s$, is nearly compensated by the interfacial perpendicular magnetic anisotropy field $2K_u/\mu_0 M_s$, with K_u the unixial magnetic anisotropy energy density. The strong variations of $H_{\mathrm{eff}} = 2K_u/\mu_0 M_s - M_s$ observed here are due to those much smaller in proportion of K_u with Ru overlayer thickness (while saturation magnetization M_s is found constant, see Supplemental Material), which may be ascribed to a combination of atomic interdiffusion and strain accumulation/relaxation effects. We highlight here that varying the Ru insertion layer thickness in Pt/Co/Ru/Pt, especially when t_{Co} is chosen not far from the spin-reorientation thickness, allows to tune precisely the effective magnetic anisotropy in the Co layer. This is of broad interest for many uses involving DMI, e.g., for controlling the formation of non-collinear magnetic textures.

The ratio D/A (or indirectly, D_s/A) also determines the energetics of non-collinear magnetic configurations in a given magnetic system. For instance, it determines the periodicity of cycloidal spin configuration orderings. The evolution of D_s/A with the thickness of the Ru insertion layer is presented in Fig. 3d. After build-up of the DMI, over which D_s/A rises sharply, the ratio slowly decreases

due to the recovery of A at larger t_{Ru}. The interplay between D, A and H_{eff}, all evolving as a function of the Ru insertion layer thickness t_{Ru}, is expected to influence strongly the formation of non-collinear magnetic textures in this system, which provides an interesting platform for magnetic textures engineering [60].

VI. FIRST-PRINCIPLES CALCULATIONS

We finally report in this last section different results from first-principles calculations of the magnetic properties in our heterostructures, in order to compare the predicted trends to our experimental results. These calculations are performed in a way very similar to several previous works [15, 16, 62], and are summarized in Figs. 4 and 5.

We first present the case of Pt/Co/Pt[t_{Pt}]/Au, corresponding to samples of section IV, beginning with the results of structural optimization performed by total-energy minimization. The relaxed configurations are obtained for different thicknesses of the insertion Pt layer, for which we compare the average interlayer spacing between atomic planes in the bottom and in the top Pt layers (Fig. 4a). A tensile strain on the top Pt layer caused by the Au layer can clearly be seen for Pt thicknesses $n \lesssim 5$ ML. With increasing thickness of the inserted Pt top layer, the tensile strain weakens gradually, and finally disappears for the Pt/Co/Pt[n=6–7 ML]/Au system. Meanwhile, the average interlayer distance between the bottom Pt planes slightly increases for Pt/Co/Pt[n=4–7 ML]/Au, as a result of the insert Pt layers. The contributions to the overall DMI energy of each atomic plane in the top Pt layer are then shown in Fig. 4b (solid lines) and compared to those of each atomic plane in the bottom Pt layer (dashed lines). Varying the top Pt thickness, we observe a modulation of the individual plane contributions in the top Pt layer. The largest contribution to the DMI comes from the Pt plane located immediately at the interface with Co. Then, the contributions from the other Pt planes decrease in absolute value with the distance away from the interface with Co, and even contribute with oscillatory sign for Pt planes $n \geq 3$. The contribution from the nearest neighbor Pt plane of Co (black line) shows a roughly linear trend with the variation of the top Pt layer thickness, whereas the contributions from the following planes tend to oscillate around the corresponding value of the DMI contribution in the bottom Pt layer (dashed lines). For $n = 7$ ML thickness in the top Pt layer, the case where both Pt layers have the same thickness and thus zero DMI would be expected in the absence of Au, a net DMI contribution remains, mainly due to the DMI imbalance considering atomic planes 1 and 2 away from the interface (see also full atomic-plane-resolved results in Supplemental Material). The evolution of the atomic-plane-resolved DMI contributions displayed in Fig. 4b shows that the Au layer influences significantly the DMI in the adjacent Pt layer, thus breaking the symmetry of the Pt/Co/Pt system. This results in an enhanced DMI in the top Pt layer compared to that in the bottom Pt layer, and therefore the total DMI of the system does not vanish. This analysis reveals that a tensile strain caused by the distant Au layer is able to modify the interfacial DMI even though the DMI energy remains localized at the Co/Pt interface, which will also apply to the deposition-induced strain found in our experiments.

We next present the results for the case of Pt/Co/Ru[t_{Ru}]/Pt, corresponding to samples of section V. We show in Fig. 5a the contributions to the overall DMI energy of each atomic plane from all layers, for Pt/Co/Ru[1]/Pt and Pt/Co/Ru[2]/Pt. These confirm two main observations made above: (i) the spin-orbit contributions to the DMI energy density at the Pt/Co interface lie mostly within the first two layers away from the interface (indexed 6,7 in Fig. 5a) and (ii) one atomic plane of Ru inserted between Co and Pt (indexed 13 in Fig. 5a) is sufficient to cancel the DMI at the Co top interface. The contributions per material layer to the overall DMI energy, as well as the overall DMI energy in Pt/Co/Ru[t_{Ru}]/Pt, are shown as a function of the number of Ru layers in Fig. 5b (see also full atomic-plane-resolved results in Supplemental Material). An increase followed by a reduction and recovery of the DMI, both around 20% of the initial value, are found when going from m=1 to 4 ML thickness in the Ru layer, which we do not observe as clearly in the experiments above. The present calculations predict the behavior of an ideal structure, with optimized parameter settings, for a specific system at low temperature. Therefore, it is expected that only a much weaker oscillation of the DMI with t_{Ru} may be found in the data shown in the inset of Fig. 3a, which is also partly hidden in the experimental measurement errors. We ascribe the evident reduction of this effect to the fact that our layers are not grown epitaxially: the small oscillating feature of Fig. 5b expected in the thickness dependence of D is likely averaged out in our sputtered multilayers by small local variations of atomic coverage at the nanometer scale. Any small intermixing between Co and Ru, which may form an alloy phase at their interface, as described above in section II, would also contribute to weaken this effect [15]. The specific oscillating feature for D predicted in Pt/Co/Ru[m=1–4 ML]/Pt could nevertheless be unambiguously observed in epitaxially grown multilayers.

We finally want to investigate on a more quantitative level how the magnetic parameters obtained from first-principles compare with our experimental results. We present in Table II the values of the main magnetic parameters in the Pt/Co/Pt, Pt/Co/Au and Pt/Co/Ru/Pt thick capping layer systems, for which computational results have been obtained within the LDA approximation. Atomistic interaction energies are converted into micromagnetic energy densities as described in Supplemental Material. In order to compare them with experiments performed at a finite temperature of 300 K, it is neces-

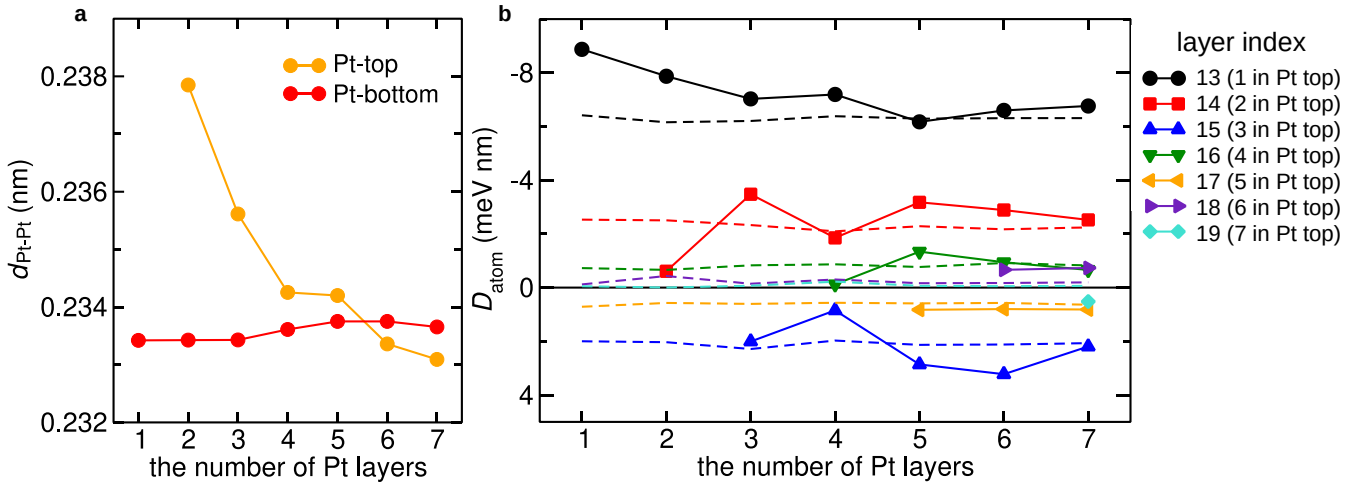

FIG. 4. First-principles predictions for the DMI in the Pt[7 ML]/Co[5 ML]/Pt[n=1–7 ML]/Au[7 ML] heterostructure. **a**. Average interlayer distance in the bottom and top Pt layers as a function of the number of top Pt ML. **b**. Evolution of the atomic-plane-resolved DMI energies, for the Pt planes adjacent and farther from Co (indexed 13 to 19, or 1 to 7 inside Pt top layer), as a function of the number of MLs in the top Pt. The top Co/Pt values (solid lines) are compared to the bottom Pt/Co ones (dotted lines). The sign of D_{atom} for top Co/Pt is inverted on this graph, to allow comparison with bottom Pt/Co.

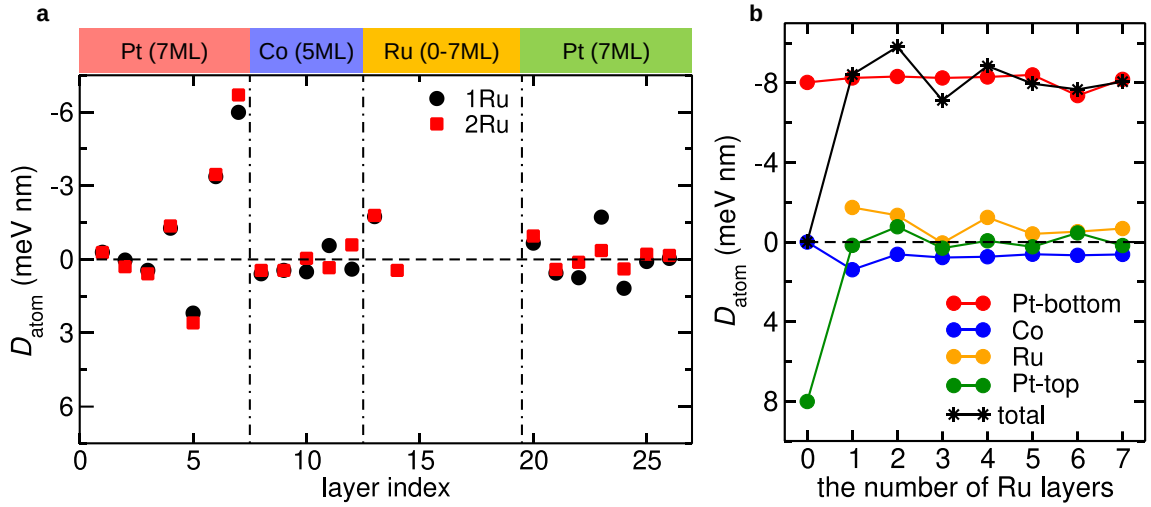

FIG. 5. First-principles predictions for the DMI in the Pt[7 ML]/Co[5 ML]/Ru[m=0–7 ML]/Pt[7 ML] heterostructure. **a**. Partial contributions from each atomic plane to the DMI energy, for the particular compositions Pt[7]/Co[5]/Ru[1]/Au[7] (black) and Pt[7]/Co[5]/Ru[2]/Au[7] (red). The computed heterostructure and its thicknesses are sketched above. **b**. Overall contribution, per material layer (the sum of the contributions from all atomic planes in this layer) to the DMI energy, as well as total DMI energy density, as a function of the number of Ru planes.

sary to take into account the rescaling of the effective magnetic parameters due to thermal effects. To do so, we infer the expected evolution with temperature of the effective magnetic parameters from that of the saturation magnetization M_s, which stems from the thermal excitation of spin-waves and can be derived from magnon statistics [63, 64]. Even at low temperatures, M_s is expected to deviate significantly from Bloch law $M_s(T) = M_0\left[1-(T/T_c)^{3/2}\right]$, where T_c is the Curie temperature and M_0 is the intrinsic spontaneous magnetization at zero temperature, due to the strong magnon confinement in the vertical direction of our nm-thin films [65]. We thus retain an experimental value of $M_s(T{=}300\,\mathrm{K})/M_0 = 0.90 \pm 0.01$, obtained by temperature-dependent SQUID magnetometry performed on our Pt/Co/Pt heterostructure. Note that in the present comparison, all magnetization values include the apparent additional magnetization of Co due to proximity effects in the neighboring Pt planes. The effective magnetic interactions are then expected to evolve with temperature following

	LDA approx. DFT (0 K)	rescaled DFT (300 K)	experimental (300 K)
Pt/Co/Pt			
M_s (MA m^{-1})	1.49	1.34	1.34 ± 0.03
A (pJ m^{-1})	32.3	26.7	25.3 ± 0.7
D_s (pJ m^{-1})	0.00	0.00	0.12 ± 0.03
K_u (MJ m^{-3})	0.61	0.28	1.06 ± 0.05
Pt/Co/Au			
M_s (MA m^{-1})	1.41	1.27	1.24 ± 0.02
A (pJ m^{-1})	32.9	27.2	25.1 ± 0.7
D_s (pJ m^{-1})	-1.24	-1.02	-1.17 ± 0.03
K_u (MJ m^{-3})	1.75	0.80	0.84 ± 0.04
Pt/Co/Ru/Pt			
M_s (MA m^{-1})	1.42	1.28	1.19 ± 0.02
A (pJ m^{-1})	30.9	25.6	23.0 ± 0.6
D_s (pJ m^{-1})	-3.08	-2.55	-1.27 ± 0.03
K_u (MJ m^{-3})	-0.16	-0.07	0.84 ± 0.04

TABLE II. Comparison between experimental and first-principles computational results. The column 'LDA approx. DFT' lists the magnetic parameters obtained from first-principles modeling, the column 'rescaled DFT' lists these values after renormalization due to temperature effects at 300 K and the column 'experimental' recaps the values presented in Table I.

power laws on M_s that can be predicted by Langevin dynamics simulations [66, 67], with A proportional to $M_s(T)^{\approx 1.8}$, D_s proportional to $M_s(T)^{\approx 1.8}$ [68] and K_u proportional to $M_s(T)^{\approx 2}$ [69], where the precise value of the exponents depend on the system geometry and type of mechanisms involved. In our comparison, we also rescale the anisotropy K_u, an effect of interfacial origin, by the ratio of thicknesses between Co[5] (or 0.96 nm) used in modeling, and Co(1.7 nm) corresponding to experiments. This is not necessary for the DMI as we consider the reduced parameter D_s. It appears from Table II that while first-principles calculations can provide a good description of magnetization, exchange and DMI interactions, it does not capture the behavior of the magnetic anisotropy in our heterostructures, which can thus only be evaluated experimentally in all cases. This can be due either to the presence of out-of-equilibrium atomic configurations at the interfaces, related to the growth by room-temperature magnetron sputtering of the successive layers, to deposition-induced strains not reflected in the crystalline ground states considered by the calculations, or to the complex temperature dependence of K_u in case of mixed anisotropies [69]. While the smaller discrepancies for A, D and M_s can be safely ascribed to imperfections in the heterostructures, it seems that the DMI in the Pt/Co/Ru system is not fully captured by the present DFT calculations, which significantly overestimate the experimental value. This is probably due to sensitivity to the exact configuration at the interfaces. Apart this specific case of interfacial D_s in Pt/Co/Ru and excluding anisotropy, which both seem beyond reach of the present models, it appears that DFT can be to a large extent reliable in predicting the amplitude of the important magnetic interactions in sputtered magnetic layers, including in some cases the DMI. This opens up exciting prospects for computational optimization of their magnetic properties.

VII. CONCLUSION

We have observed that within the realm of sputtered heterostructures and multilayers, two atomic planes of Pt are already able to bring most of the expected DMI at an interface with Co. A single atomic plane of Ru is enough to suppress DMI between Co and Pt. These results overall suggest the absence of distant spin-orbit effects on the interfacial DMI energies, implying only weak contributions to the DMI energy of atoms located beyond the second atomic plane off the interface, in agreement with first-principles calculations that we have revisited for our specific system. This points towards a local electronic mechanism responsible for the generation of DMI at interfaces with an FM [33, 41], at least concerning combinations of metals similar to Pt and Ru with Co. This shall be useful for identifying the actual mechanism causing interfacial DMI in thin layers of itinerant ferromagnets, as opposed to the well-known Fert-Levy mechanism causing DMI in diluted magnetic alloys doped with impurities. Our results provide support for the explanation involving interfacial electric fields induced by charge redistribution across the interface [17]. Similar investigations for other metals also generating measurable interfacial DMI (such as Ta or W, interfaced with Co or Fe) would be much appreciable to confirm this result and improve this understanding, as well as on what determines the characteristic lengthscale for interfacial DMI build-up. Further, our results confirm several clues of a distant modulation of the interfacial DMI by strain effects under the influence of above-deposited layers, such as the observation of a larger DMI strength at top Co/Pt than at bottom Pt/Co interface, and that the DMI does not remain constant upon the addition of subsequent Pt planes. This explanation is also supported by first-principles modeling. This extrinsic modulation mechanism is not to be confused with a direct electronic effect that would be

caused by these additional atomic planes.

Further consideration of the local aspect of the electronic mechanisms giving rise to the interfacial DMI, which can nevertheless be modulated by strain engineering, shall be easily combined with the findings of other works dealing with the same Pt/Co platform, such as predictions of a consequent modulation of the DMI by non-magnetic metals nearby Pt, in case of atomically thin layers with sharp interfaces [62]. The present observations also open new prospects for obtaining a strong DMI in sputtered multilayers made of repeats of very thin layers [70], as well as they allow for an engineering of the DMI by the insertion of dusting layers well below 1 nm [44], within multilayers optimized for other properties, e.g., magnetic anisotropy or spin-orbit torques.

ACKNOWLEDGMENTS

A. T. thanks V. Demidov (Muenster University, Germany) for advice in the initial setup, and the mechanical workshop of LPS, especially S. Cabaret, for the design and fabrication of numerous mechanical parts for the experiment. We are grateful to N. Brun for the help in analyzing the STEM-EELS measurement data. We thank A. Fert for precious advice and several discussions about DMI. PhOM and EOE departments from Univ. Paris-Saclay, CNRS INP, the Sesame Ile de France IMAGeSPIN project (No. EX039175) and the French National Research Agency as part of the "Investissements d'Avenir" program by LABEX NanoSaclay (No. ANR-10-LABX-0035, BLS@PSay and SPiCY projects) are acknowledged for the BLS equipment purchase. We acknowledge financial support from the Agence Nationale de la Recherche, France, under grant agreement No. ANR-17-CE24-0025 (TOPSKY), from the DARPA TEE program, through grant MIPR No. HR0011831554, and from the Horizon2020 Framework Program of the European Commission, under FET-Proactive Grant agreement No. 824123 (SKYTOP). We acknowledge funding from the French National Research Agency under the "Investissements d'Avenir" program TEMPOS (No. ANR-10-EQPX-50) for FIB access.

[1] A. Fert and P. M. Levy, Role of Anisotropic Exchange Interactions in Determining the Properties of Spin-Glasses, Phys. Rev. Lett. **44**, 1538 (1980).
[2] A. Fert, Magnetic and Transport Properties of Metallic Multilayers, in *Metallic Multilayers*, Vol. 59–60 (Trans Tech Publications, 1990) pp. 439–480.
[3] I. Dzyaloshinsky, A thermodynamic theory of "weak" ferromagnetism of antiferromagnetics, J. Phys. Chem. Solids **4**, 241 (1958).
[4] T. Moriya, Anisotropic Superexchange Interaction and Weak Ferromagnetism, Phys. Rev. **120**, 91 (1960).
[5] A. Crépieux and C. Lacroix, Dzyaloshinsky–Moriya interactions induced by symmetry breaking at a surface, J. Magn. Magn. Mater. **182**, 341 (1998).
[6] M. Bode, M. Heide, K. von Bergmann, P. Ferriani, S. Heinze, G. Bihlmayer, A. Kubetzka, O. Pietzsch, S. Blügel, and R. Wiesendanger, Chiral magnetic order at surfaces driven by inversion asymmetry, Nature **447**, 190 (2007).
[7] M. Heide, G. Bihlmayer, and S. Blügel, Dzyaloshinskii-Moriya interaction accounting for the orientation of magnetic domains in ultrathin films: Fe/W(110), Phys. Rev. B **78**, 140403(R) (2008).
[8] A. Thiaville, S. Rohart, É. Jué, V. Cros, and A. Fert, Dynamics of Dzyaloshinskii domain walls in ultrathin magnetic films, Europhys. Lett. **100**, 57002 (2012).
[9] F. Büttner, I. Lemesh, and G. S. D. Beach, Theory of isolated magnetic skyrmions: From fundamentals to room temperature applications, Sci. Rep. **8**, 4464 (2018).
[10] J. Sampaio, A. V. Khvalkovskiy, M. Kuteifan, M. Cubukcu, D. Apalkov, V. Lomakin, V. Cros, and N. Reyren, Disruptive effect of Dzyaloshinskii-Moriya interaction on the magnetic memory cell performance, Appl. Phys. Lett. **108**, 112403 (2016).
[11] L. Caretta, M. Mann, F. Büttner, K. Ueda, B. Pfau, C. M. Günther, P. Hessing, A. Churikova, C. Klose, M. Schneider, D. Engel, C. Marcus, D. Bono, K. Bagschik, S. Eisebitt, and G. S. D. Beach, Fast current-driven domain walls and small skyrmions in a compensated ferrimagnet, Nat. Nanotechnol. **13**, 1154 (2018).
[12] Z. Luo, T. P. Dao, A. Hrabec, J. Vijayakumar, A. Kleibert, M. Baumgartner, E. Kirk, J. Cui, T. Savchenko, G. Krishnaswamy, L. J. Heyderman, and P. Gambardella, Chirally coupled nanomagnets, Science **363**, 1435 (2019).
[13] H. Yang, A. Thiaville, S. Rohart, A. Fert, and M. Chshiev, Anatomy of Dzyaloshinskii-Moriya Interaction at Co / Pt Interfaces, Phys. Rev. Lett. **115**, 267210 (2015).
[14] A. Belabbes, G. Bihlmayer, F. Bechstedt, S. Blügel, and A. Manchon, Hund's Rule-Driven Dzyaloshinskii-Moriya Interaction at 3d-5d Interfaces, Phys. Rev. Lett. **117**, 247202 (2016).
[15] B. Zimmermann, W. Legrand, D. Maccariello, N. Reyren, V. Cros, S. Blügel, and A. Fert, Dzyaloshinskii-Moriya interaction at disordered interfaces from ab initio theory: Robustness against intermixing and tunability through dusting, Appl. Phys. Lett. **113**, 232403 (2018).
[16] H. Jia, B. Zimmermann, and S. Blügel, First-principles investigation of chiral magnetic properties in multilayers: Rh/Co/Pt and Pd/Co/Pt, Phys. Rev. B **98**, 144427 (2018).
[17] H. Jia, B. Zimmermann, G. Michalicek, G. Bihlmayer, and S. Blügel, Electric dipole moment as descriptor for interfacial Dzyaloshinskii-Moriya interaction, Phys. Rev. Mater. **4**, 024405 (2020).
[18] M. Kuepferling, A. Casiraghi, G. Soares, G. Durin, F. Garcia-Sanchez, L. Chen, C. H. Back, C. H. Marrows, S. Tacchi, and G. Carlotti, Measuring interfacial Dzyaloshinskii-Moriya interaction in ultra thin films,

arXiv:2009.11830v2 [cond-mat.mes-hall] (2020).

[19] J. Cho, N.-H. Kim, S. Lee, J.-S. Kim, R. Lavrijsen, A. Solignac, Y. Yin, D.-S. Han, N. J. J. van Hoof, H. J. M. Swagten, B. Koopmans, and C.-Y. You, Thickness dependence of the interfacial Dzyaloshinskii–Moriya interaction in inversion symmetry broken systems, Nat. Commun. **6**, 7635 (2015).

[20] M. Belmeguenai, J.-P. Adam, Y. Roussigné, S. Eimer, T. Devolder, J.-V. Kim, S. M. Cherif, A. Stashkevich, and A. Thiaville, Interfacial Dzyaloshinskii-Moriya interaction in perpendicularly magnetized Pt/Co/AlO_x ultrathin films measured by Brillouin light spectroscopy, Phys. Rev. B **91**, 180405(R) (2015).

[21] K. Di, V. L. Zhang, H. S. Lim, S. C. Ng, M. H. Kuok, J. Yu, J. Yoon, X. Qiu, and H. Yang, Direct Observation of the Dzyaloshinskii-Moriya Interaction in a Pt/Co/Ni Film, Phys. Rev. Lett. **114**, 047201 (2015).

[22] H. T. Nembach, J. M. Shaw, M. Weiler, E. Jué, and T. J. Silva, Linear relation between Heisenberg exchange and interfacial Dzyaloshinskii–Moriya interaction in metal films, Nat. Phys. **11**, 825 (2015).

[23] R. Soucaille, M. Belmeguenai, J. Torrejon, J.-V. Kim, T. Devolder, Y. Roussigné, S.-M. Chérif, A. A. Stashkevich, M. Hayashi, and J.-P. Adam, Probing the Dzyaloshinskii-Moriya interaction in CoFeB ultrathin films using domain wall creep and Brillouin light spectroscopy, Phys. Rev. B **94**, 104431 (2016).

[24] E. C. Corredor, S. Kuhrau, F. Kloodt-Twesten, R. Frömter, and H. P. Oepen, SEMPA investigation of the Dzyaloshinskii-Moriya interaction in the single, ideally grown Co/Pt(111) interface, Phys. Rev. B **96**, 060410(R) (2017).

[25] N.-H. Kim, D.-S. Han, J. Jung, K. Park, H. J. M. Swagten, J.-S. Kim, and C.-Y. You, Dependence of interfacial Dzyaloshinskii–Moriya interaction and perpendicular magnetic anisotropy on the thickness of the heavy-metal layer, Appl. Phys. Express **10**, 103003 (2017).

[26] R. M. Rowan-Robinson, A. A. Stashkevich, Y. Roussigné, M. Belmeguenai, S.-M. Chérif, A. Thiaville, T. P. A. Hase, A. T. Hindmarch, and D. Atkinson, The interfacial nature of proximity-induced magnetism and the Dzyaloshinskii-Moriya interaction at the Pt/Co interface, Sci. Rep. **7**, 16835 (2017).

[27] S. Tacchi, R. E. Troncoso, M. Ahlberg, G. Gubbiotti, M. Madami, J. Åkerman, and P. Landeros, Interfacial Dzyaloshinskii-Moriya Interaction in Pt/CoFeB Films: Effect of the Heavy-Metal Thickness, Phys. Rev. Lett. **118**, 147201 (2017).

[28] A. W. J. Wells, P. M. Shepley, C. H. Marrows, and T. A. Moore, Effect of interfacial intermixing on the Dzyaloshinskii-Moriya interaction in Pt/Co/Pt, Phys. Rev. B **95**, 054428 (2017).

[29] S. Kim, K. Ueda, G. Go, P.-H. Jang, K.-J. Lee, A. Belabbes, A. Manchon, M. Suzuki, Y. Kotani, T. Nakamura, K. Nakamura, T. Koyama, D. Chiba, K. T. Yamada, D.-H. Kim, T. Moriyama, K.-J. Kim, and T. Ono, Correlation of the Dzyaloshinskii–Moriya interaction with Heisenberg exchange and orbital asphericity, Nat. Commun. **9**, 1648 (2018).

[30] G. W. Kim, A. S. Samardak, Y. J. Kim, I. H. Cha, A. V. Ognev, A. V. Sadovnikov, S. A. Nikitov, and Y. K. Kim, Role of the Heavy Metal's Crystal Phase in Oscillations of Perpendicular Magnetic Anisotropy and the Interfacial Dzyaloshinskii-Moriya Interaction in W/Co-Fe-B/MgO Films, Phys. Rev. Appl. **9**, 064005 (2018).

[31] X. Ma, G. Yu, C. Tang, X. Li, C. He, J. Shi, K. L. Wang, and X. Li, Interfacial Dzyaloshinskii-Moriya Interaction: Effect of 5*d* Band Filling and Correlation with Spin Mixing Conductance, Phys. Rev. Lett. **120**, 157204 (2018).

[32] A. K. Chaurasiya, S. Choudhury, J. Sinha, and A. Barman, Dependence of Interfacial Dzyaloshinskii-Moriya Interaction on Layer Thicknesses in Ta/Co-Fe-B/TaOx Heterostructures from Brillouin Light Scattering, Phys. Rev. Appl. **9**, 014008 (2018).

[33] Y.-K. Park, D.-Y. Kim, J.-S. Kim, Y.-S. Nam, M.-H. Park, H.-C. Choi, B.-C. Min, and S.-B. Choe, Experimental observation of the correlation between the interfacial Dzyaloshinskii–Moriya interaction and work function in metallic magnetic trilayers, NPG Asia Mater. **10**, 995 (2018).

[34] K. Shahbazi, A. Hrabec, S. Moretti, M. B. Ward, T. A. Moore, V. Jeudy, E. Martinez, and C. H. Marrows, Magnetic properties and field-driven dynamics of chiral domain walls in epitaxial Pt/Co/Au_xPt_{1-x} trilayers, Phys. Rev. B **98**, 214413 (2018).

[35] M. Baćani, M. A. Marioni, J. Schwenk, and H. J. Hug, How to measure the local Dzyaloshinskii-Moriya Interaction in Skyrmion Thin-Film Multilayers, Sci. Rep. **9**, 3114 (2019).

[36] W. Zhang, B. Jiang, L. Wang, Y. Fan, Y. Zhang, S. Y. Yu, G. B. Han, G. L. Liu, C. Feng, G. H. Yu, S. S. Yan, and S. Kang, Enhancement of Interfacial Dzyaloshinskii-Moriya Interaction: A Comprehensive Investigation of Magnetic Dynamics, Phys. Rev. Appl. **12**, 064031 (2019).

[37] N. S. Gusev, A. V. Sadovnikov, S. A. Nikitov, M. V. Sapozhnikov, and O. G. Udalov, Manipulation of the Dzyaloshinskii–Moriya Interaction in Co/Pt Multilayers with Strain, Phys. Rev. Lett. **124**, 157202 (2020).

[38] M. Arora, J. M. Shaw, and H. T. Nembach, Variation of sign and magnitude of the Dzyaloshinskii-Moriya interaction of a ferromagnet with an oxide interface, Phys. Rev. B **101**, 054421 (2020).

[39] H. T. Nembach, E. Jué, E. R. Evarts, and J. M. Shaw, Correlation between Dzyaloshinskii-Moriya interaction and orbital angular momentum at an oxide-ferromagnet interface, Phys. Rev. B **101**, 020409(R) (2020).

[40] Y.-K. Park, J.-S. Kim, Y.-S. Nam, S. Jeon, J.-H. Park, K.-W. Kim, H.-W. Lee, B.-C. Min, and S.-B. Choe, Interfacial atomic layers for full emergence of interfacial Dzyaloshinskii–Moriya interaction, NPG Asia Materials **12**, 38 (2020).

[41] F. Ajejas, Y. Sassi, W. Legrand, S. Collin, A. Thiaville, J. P. Garcia, S. Pizzini, N. Reyren, V. Cros, and A. Fert, Element-selective modulation of interfacial Dzyaloshinskii-Moriya interaction in Pt—Co—Metal based multilayers, arXiv:2109.00761 [cond-mat.mtrl-sci] (2021).

[42] A. Soumyanarayanan, M. Raju, A. L. G. Oyarce, A. K. C. Tan, M.-Y. Im, A. P. Petrović, P. Ho, K. H. Khoo, M. Tran, C. K. Gan, F. Ernult, and C. Panagopoulos, Tunable room-temperature magnetic skyrmions in Ir/Fe/Co/Pt multilayers, Nat. Mater. **16**, 898 (2017).

[43] H. Yang, G. Chen, A. A. C. Cotta, A. T. N'Diaye, S. A. Nikolaev, E. A. Soares, W. A. A. Macedo, K. Liu, A. K. Schmid, A. Fert, and M. Chshiev, Significant Dzyaloshinskii–Moriya interaction at graphene–ferromagnet interfaces due to the Rashba effect, Nat. Mater. **17**, 605 (2018).

[44] R. Tolley, S. A. Montoya, and E. E. Fullerton, Room-temperature observation and current control of skyrmions in Pt/Co/Os/Pt thin films, Phys. Rev. Mater. **2**, 044404 (2018).

[45] C. Xu, J. Feng, S. Prokhorenko, Y. Nahas, H. Xiang, and L. Bellaiche, Topological spin texture in Janus monolayers of the chromium trihalides Cr(I, X)$_3$, Phys. Rev. B **101**, 060404(R) (2020).

[46] J. Liang, W. Wang, H. Du, A. Hallal, K. Garcia, M. Chshiev, A. Fert, and H. Yang, Very large Dzyaloshinskii-Moriya interaction in two-dimensional Janus manganese dichalcogenides and its application to realize skyrmion states, Phys. Rev. B **101**, 184401 (2020).

[47] H. Yang, O. Boulle, V. Cros, A. Fert, and M. Chshiev, Controlling Dzyaloshinskii-Moriya Interaction via Chirality Dependent Atomic-Layer Stacking, Insulator Capping and Electric Field, Sci. Rep. **8**, 12356 (2018).

[48] A. Hrabec, M. Belmeguenai, A. Stashkevich, S. M. Chérif, S. Rohart, Y. Roussigné, and A. Thiaville, Making the Dzyaloshinskii-Moriya interaction visible, Appl. Phys. Lett. **110**, 242402 (2017).

[49] J.-H. Moon, S.-M. Seo, K.-J. Lee, K.-W. Kim, J. Ryu, H.-W. Lee, R. D. McMichael, and M. D. Stiles, Spin-wave propagation in the presence of interfacial Dzyaloshinskii-Moriya interaction, Phys. Rev. B **88**, 184404 (2013).

[50] B. A. Kalinikos, Spectrum and linear excitation of spin waves in ferromagnetic films, Sov. Phys. J. **24**, 718 (1981).

[51] T. Böttcher, K. Lee, F. Heussner, S. Jaiswal, G. Jakob, M. Kläui, B. Hillebrands, T. Brächer, and P. Pirro, Heisenberg Exchange and Dzyaloshinskii-Moriya Interaction in Ultrathin CoFeB Single and Multilayers, arXiv:2006.02690v1 [cond-mat.mtrl-sci] (2020).

[52] G. Kresse and J. Furthmüller, Efficiency of ab-initio total energy calculations for metals and semiconductors using a plane-wave basis set, Comput. Mater. Sci. **6**, 15 (1996).

[53] G. Kresse and J. Hafner, Ab initio molecular-dynamics simulation of the liquid-metal–amorphous-semiconductor transition in germanium, Phys. Rev. B **49**, 14251 (1994).

[54] J. P. Perdew, K. Burke, and M. Ernzerhof, Generalized Gradient Approximation Made Simple, Phys. Rev. Lett. **77**, 3865 (1996).

[55] J. P. Perdew and A. Zunger, Self-interaction correction to density-functional approximations for many-electron systems, Phys. Rev. B **23**, 5048 (1981).

[56] For the program description, see `http://www.flapw.de`.

[57] M. Heide, G. Bihlmayer, and S. Blügel, Describing Dzyaloshinskii–Moriya spirals from first principles, J. Phys. B **404**, 2678 (2009).

[58] B. Zimmermann, M. Heide, G. Bihlmayer, and S. Blügel, First-principles analysis of a homochiral cycloidal magnetic structure in a monolayer Cr on W(110), Phys. Rev. B **90**, 115427 (2014).

[59] C. Eyrich, A. Zamani, W. Huttema, M. Arora, D. Harrison, F. Rashidi, D. Broun, B. Heinrich, O. Mryasov, M. Ahlberg, O. Karis, P. E. Jönsson, M. From, X. Zhu, and E. Girt, Effects of substitution on the exchange stiffness and magnetization of Co films, Phys. Rev. B **90**, 235408 (2014).

[60] W. Legrand, D. Maccariello, F. Ajejas, S. Collin, A. Vecchiola, K. Bouzehouane, N. Reyren, V. Cros, and A. Fert, Room-temperature stabilization of antiferromagnetic skyrmions in synthetic antiferromagnets, Nat. Mater. **19**, 34 (2020).

[61] S. D. Pollard, J. A. Garlow, J. Yu, Z. Wang, Y. Zhu, and H. Yang, Observation of stable Néel skyrmions in cobalt/palladium multilayers with Lorentz transmission electron microscopy, Nat. Commun. **8**, 14761 (2017).

[62] H. Jia, B. Zimmermann, M. Hoffmann, M. Sallermann, G. Bihlmayer, and S. Blügel, Material systems for FM-/AFM-coupled skyrmions in Co/Pt-based multilayers, Phys. Rev. Mater. **4**, 094407 (2020).

[63] M. D. Kuz'min, Shape of Temperature Dependence of Spontaneous Magnetization of Ferromagnets: Quantitative Analysis, Phys. Rev. Lett. **94**, 107204 (2005).

[64] R. F. L. Evans, U. Atxitia, and R. W. Chantrell, Quantitative simulation of temperature-dependent magnetization dynamics and equilibrium properties of elemental ferromagnets, Phys. Rev. B **91**, 144425 (2015).

[65] I. A. Yastremsky, O. M. Volkov, M. Kopte, T. Kosub, S. Stienen, K. Lenz, J. Lindner, J. Fassbender, B. A. Ivanov, and D. Makarov, Thermodynamics and Exchange Stiffness of Asymmetrically Sandwiched Ultrathin Ferromagnetic Films with Perpendicular Anisotropy, Phys. Rev. Appl. **12**, 064038 (2019).

[66] R. Moreno, R. F. L. Evans, S. Khmelevskyi, M. C. Muñoz, R. W. Chantrell, and O. Chubykalo-Fesenko, Temperature-dependent exchange stiffness and domain wall width in Co, Phys. Rev. B **94**, 104433 (2016).

[67] H. Sato, P. Chureemart, F. Matsukura, R. W. Chantrell, H. Ohno, and R. F. L. Evans, Temperature-dependent properties of CoFeB/MgO thin films: Experiments versus simulations, Phys. Rev. B **98**, 214428 (2018).

[68] Y. Zhou, R. Mansell, S. Valencia, F. Kronast, and S. van Dijken, Temperature dependence of the Dzyaloshinskii-Moriya interaction in ultrathin films, Phys. Rev. B **101**, 054433 (2020).

[69] R. F. L. Evans, L. Rózsa, S. Jenkins, and U. Atxitia, Temperature scaling of two-ion anisotropy in pure and mixed anisotropy systems, Phys. Rev. B **102**, 020412(R) (2020).

[70] W. S. Ham, A.-M. Pradipto, K. Yakushiji, K. Kim, S. H. Rhim, K. Nakamura, Y. Shiota, S. Kim, and T. Ono, Dzyaloshinskii–Moriya interaction in noncentrosymmetric superlattices, npj Comput. Mater. **7**, 129 (2021).